J. Fluid Mech. (1981), *vol.* 104, *pp.* 93–109
Printed in Great Britain

The use of dual heat injection to infer scalar covariance decay in grid turbulence

By Z. WARHAFT

Sibley School of Mechanical and Aerospace Engineering,
Cornell University, Ithaca, New York 14853

(Received 15 January 1980 and in revised form 27 March 1980)

Thermal fluctuations introduced into decaying grid turbulence at two different downstream locations are shown to be initially correlated and this correlation decays with distance from the grid. The fluctuations are introduced by placing two *mandolines* (Warhaft & Lumley 1978) at different distances downstream from the grid. The sum of the thermal variances produced by each *mandoline* operating separately, $\overline{\theta_1^2}+\overline{\theta_2^2}$, is significantly less than the total variance produced by both *mandolines* operating simultaneously, $\overline{(\theta_1+\theta_2)^2} = \overline{\theta_1^2}+\overline{\theta_2^2}+2\overline{\theta_1\theta_2}$, i.e. the deficit is due to the covariance term $2\overline{\theta_1\theta_2}$. This covariance is responsible for a cross-correlation, $\rho = \overline{\theta_1\theta_2}/(\overline{\theta_1^2}\overline{\theta_2^2})^{\frac{1}{2}}$, as great as 0·6. The decay of $\overline{\theta_1\theta_2}$ and ρ is studied for various initial input thermal scale sizes and for various input locations. It is shown that the covariance follows a power-law decay, the exponent varying from $-5{\cdot}5$ if the thermal fluctuations are introduced close to the grid where the turbulence dissipation rate is large and the flow is inhomogeneous to -4 if they are introduced further downstream ($x/M \geqslant 10$, where x is the distance from the grid and M is the grid mesh length) in the region where the approximately isotropic turbulence is beginning to develop. The decay rate of $\overline{\theta_1\theta_2}$ and ρ was insensitive to the intensity of the thermal fluctuations. In all these experiments the cross-correlation between velocity and temperature fluctuations was very small ($\sim -0{\cdot}05$) and temperature was a passive additive. The results, which appear to be the first quantitative measurements of the rate of destruction of scalar covariance and hence of the mixing rate between two scalars, are shown to provide good confirmation of recent predictions of the decay of ρ by the second-order closure techniques of Lumley (1978*a*, *b*).

1. Introduction

A principal characteristic of turbulence, and one that has provided impetus for much turbulence research, is its ability to mix and to transport rapidly heat and scalars such as moisture, chemical reactants, pollutants and ions, as well as many others. Often, both in nature and in the laboratory, two scalars are involved in the mixing and transport process. For example, in the atmosphere there are usually both temperature and humidity fluctuations and the question arises as to what effect the fluctuations and gradients of one scalar may have on the transport of the other (Warhaft 1976). Further, the radio refractive index is a function of both temperature and humidity fluctuations and thus the temperature–humidity covariance plays a role in determining

0022-1120/81/4640-3310 $02.00

the scattering of electromagnetic waves (Wyngaard *et al.* 1978). In order to understand these processes knowledge is required of the cross-correlation between the temperature and humidity fluctuations and how this varies both spatially and temporally. Further examples of the mixing of two scalars may be drawn from the oceans where there are temperature and salinity fluctuations, the upper atmosphere where various ions are mixed as well as plasma mixing in stars and nebulae. But perhaps the most significant processes involving the mixing of two scalars are those in which fast chemical reactions occur. Here one of the vital parameters determining the reaction rate is the rate at which the two scalars are mixed together and smeared at the Kolmogorov microscale where the reaction takes place (Corrsin 1961; Hill 1976; Libby & Williams 1976).

In spite of the importance of two-scalar mixing there appears to be no quantitative data on their mixing rate even for passive, non-reactive scalars in simple flows. It is the purpose of this study to examine this problem experimentally for grid-generated turbulent flow, a flow that is not only of academic importance because of its comparative simplicity, but also of practical significance since it is paradigmatic of many situations in which two scalars are mixed (Libby & Williams 1976).

The rate equation for the covariance of two scalars is

$$\frac{\partial\overline{\alpha\beta}}{\partial t}+U_j\frac{\partial\overline{\alpha\beta}}{\partial x_j}+\frac{\partial A}{\partial x_j}\overline{\beta u_j}+\frac{\partial B}{\partial x_j}\overline{\alpha u_j}+\frac{\partial\overline{\alpha\beta u_j}}{\partial x_j}=-(\kappa_1+\kappa_2)\overline{\frac{\partial\alpha}{\partial x_j}\frac{\partial\beta}{\partial x_j}}, \tag{1}$$

where α and β are the fluctuations of the two scalars which have respective means A and B, U_j and u_j are the mean and fluctuating components of velocity and κ_1 and κ_2 are the molecular (or thermal, in the case of temperature) diffusivities of A and B. The overbars denote averaging. This equation is derived in a similar manner to that for the scalar variance except here the equation for α is multiplied by β and that for β is multiplied by α and the two resulting equations are added and averaged; equation 1 then results after making the usual assumptions for high-Reynolds-number turbulence (Tennekes & Lumley 1972). For decaying grid-generated turbulence in which there are fluctuations of α and β but no mean gradients of these quantities, equation (1) reduces to

$$\frac{\partial\overline{\alpha\beta}}{\partial t}=-(\kappa_1+\kappa_2)\overline{\frac{\partial\alpha}{\partial x_j}\frac{\partial\beta}{\partial x_j}}. \tag{2}$$

The term on the right-hand side of equation (2) is the dissipation rate of the scalar covariance and is often denoted as $\epsilon_{\alpha\beta}$. Equation (2) describes the rate at which the scalar covariance is destroyed and thus the rate at which the scalars are smeared and mixed at the microscale, and has obvious significance in determining chemical reaction rates and combustion rates.

In this work a simple approach will be taken for the study of equation (2). A single scalar (temperature) will be introduced at two different locations (and generally at different scales) into decaying grid turbulence. We will show by a method of inference that the two sets of temperature fluctuations, θ_1 and θ_2, are initially correlated, giving rise to a covariance $\overline{\theta_1\theta_2}$, and that as the flow evolves this covariance is dissipated. Thus for our study $\kappa_1=\kappa_2=\kappa$, the thermal diffusivity, and the governing equation is

$$\frac{\partial\overline{\theta_1\theta_2}}{\partial t}=-2\kappa\overline{\frac{\partial\theta_1}{\partial x_j}\frac{\partial\theta_2}{\partial x_j}}. \tag{3}$$

It should be noted that, in most problems involving gaseous mixing, $\kappa_1\sim\kappa_2$.

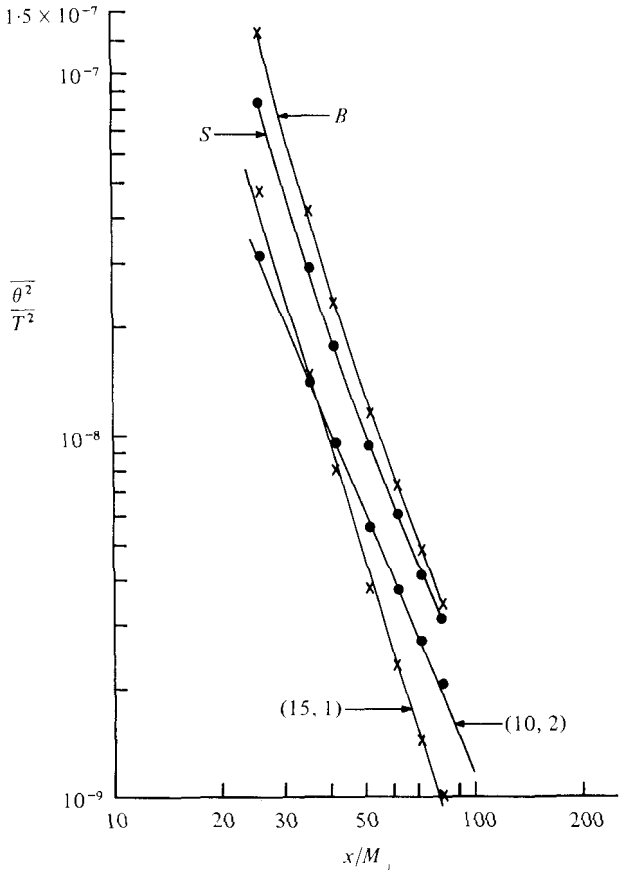

FIGURE 1. The two lower curves are the thermal variance decays for each *mandoline* operating separately; the *mandoline* configurations are (10, 2) and (15, 1) (see text for nomenclature). Curve S is the sum of the two lower curves and curve B is the variance decay for both *mandolines* operating simultaneously. T, the mean temperature, is 300 °K and x/M is the normalized downstream distance (M is the mesh length, 2·5 cm).

2. Apparatus

The experiments were conducted in the same vertically oriented wind tunnel as used by Warhaft (1980) but with a constant-area test section rather than with the secondary contraction used in the previous study. Thus the tunnel had a 16 × 16 mesh length cross-section and a streamwise extent of 180 mesh lengths, where the mesh length (M) of the biplanar turbulence-generating grid was 0·025 m and its solidity was 0·34. The mean speed was 6·4 m s^{-1}. As in Warhaft & Lumley (1978) and Warhaft (1980) temperature fluctuations were generated by means of a *mandoline*: fine heated wires in a parallel planar array placed perpendicular to the flow downstream from the grid. The actual *mandoline* configurations employed will be described in the next section. It was experimentally determined that the *mandolines* had no effect on either the velocity spectra or on the velocity variance decay rate even when two mandolines were placed in the flow as was the case for the experiments to be described here. For further discussion of the effect of the *mandolines* on the velocity field see Warhaft (1980).

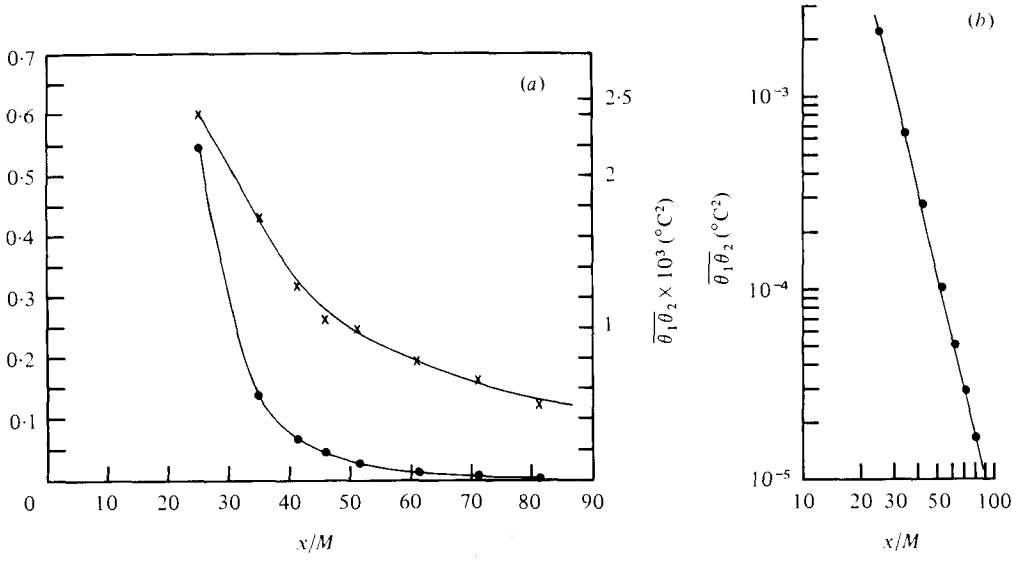

FIGURE 2. (*a*) The decay of ρ (crosses) and scalar covariance (dots) for the data of figure 1 plotted as a function of x/M. (*b*) The decay of the scalar covariance of (*a*) plotted on logarithmic co-ordinates.

Temperature and velocity fluctuations were measured using the same instrumentation as in Warhaft (1980). The noise measured by the resistance thermometer when placed in the wind tunnel operating without current being fed through *mandolines* was approximately 4×10^{-3} °C. The data acquisition and analysis system was also the same as that used by Warhaft (1980) but here we will present un-smoothed spectra computed from 5×10^5 data points.

3. Method

In Warhaft & Lumley (1978) and Warhaft (1980) it was shown that the decay rate of temperature variance in grid-generated turbulence is a function of the initial scale size of the scalar relative to the velocity field. By either moving the *mandoline* away from the grid or by decreasing the spacing between the *mandoline* wires the thermal scale was decreased relative to that of the velocity scale and thus the thermal variance decay rate was increased.

In this experiment two mandolines were placed at different locations downstream from the grid. The total temperature variance downstream from the *mandolines* is

$$\overline{(\theta_1+\theta_2)^2} = \overline{\theta_1^2}+\overline{\theta_2^2}+2\overline{\theta_1\theta_2}, \tag{4}$$

where θ_1 and θ_2 are the fluctuations produced by each *mandoline*.

We will consider first an experiment in which the *mandolines* were placed at (10, 2) and (15, 1) where, in the notation of Warhaft (1980), the first term in parenthesis denotes the distance of the *mandoline* from the grid and the second term is the distance between the *mandoline* wires. The units are in grid mesh lengths. Figure 1 shows the temperature variance decay for each *mandoline* heated separately, their sum (curve *S*) and the total variance when both *mandolines* are heated together (curve *B*). For the

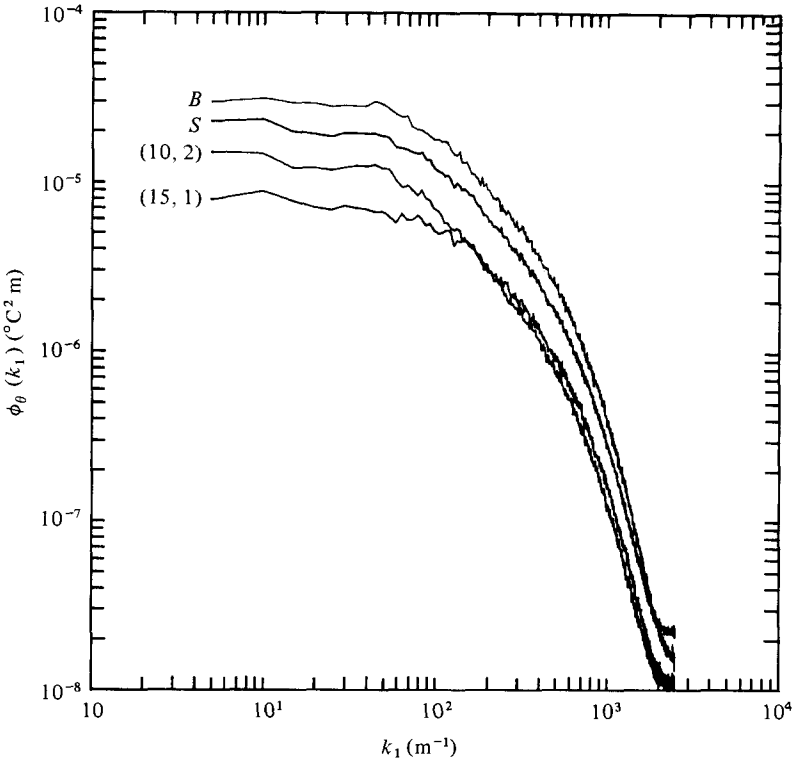

FIGURE 3. Power spectra measured at $x/M = 35$ for the data of figure 1. The two lower curves are the spectra for each *mandoline* operating separately, curve S is their sum and curve B is the power spectrum for both *mandolines* operating simultaneously.

latter case the variance is greater than the sum of the individual variances (curve S) by nearly 60 % at $x/M = 27$, a value far in excess of that which could be attributed to experimental error (5 % at most). From equation (4) this extra variance is identified as the scalar covariance term, $2\overline{\theta_1\theta_2}$. Figure 2($a$) shows a plot of this covariance, derived from the data of figure 1 by subtracting curve S from curve B and dividing by 2 (equation (4)), plotted as a function of x/M. The covariance decays rapidly, following a power-law decay (as do the individual variances) but with a much higher exponent as can be seen if $\overline{\theta_1\theta_2}$ is plotted in logarithmic co-ordinates, figure 2(b). The slope is -4. Figure 2(a) also shows a plot of the decay of the cross-correlation coefficient, ρ, between θ_1 and θ_2 defined as

$$\rho \equiv \overline{\theta_1\theta_2}/(\overline{\theta_1^2}\,\overline{\theta_2^2})^{\frac{1}{2}}.$$

The cross-correlation decreases monotonically from an initially high value of 0·6 at $x/M = 27$ to a value of 0·12 at $x/M = 81$.

The form of these results is in accord with expectation. Thus ρ should be positive since the velocity eddy turn-over time is much longer than the time it takes the velocity field to move from the first to the second *mandoline* and hence θ_1 and θ_2 will be 'turned over' in the same way, i.e. they will be positively correlated. Also, we would expect $\overline{\theta_1\theta_2}$ to decay more rapidly than the individual variances since both variance decay and a decoupling of the two fields are involved in the covariance decay.

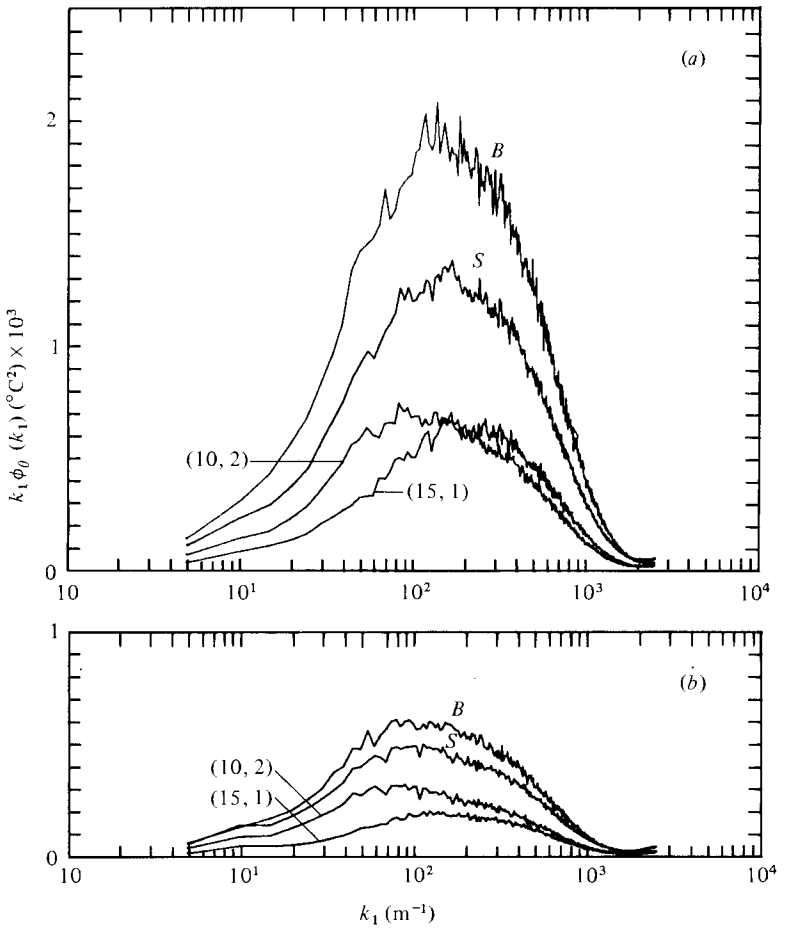

FIGURE 4. Power spectra for the data of figure 1 multiplied by k. (*a*) $x/M = 35$. (*b*) $x/m = 46$. The notation is the same as that for figure 3.

We note that extreme care was taken in measuring the variances of figure 1 and the experiments to follow: the probe was placed at a particular location in the flow, the temperature variance was measured with one *mandoline* operating, then with the other and then with both together. The tunnel was kept running throughout the measurements and because of the low power in the mandolines (a few hundred watts; see Warhaft 1980) the mean air temperature (approximately 300 K) did not change nor did the mean wind speed. The noise of the resistance thermometer and wind tunnel was measured for each variance decay and was subtracted from the measured variances on a mean square basis. The temperature fluctuations were passive for all the measurements reported here. The temperature–velocity cross-correlation was deliberately kept at a low value by having low current in the *mandolines*, it was generally $-0{\cdot}05$ and never greater than $-0{\cdot}1$.† Thus, $\overline{u_1\theta_1} \sim \overline{u_2\theta_2} \sim 0$. If this were not the case, the simple

† The negative correlation is caused by the small velocity deficit behind the heated *mandoline* wires. This velocity deficit is too small, however, to significantly influence the velocity variance. The previous explanation for this correlation (Warhaft 1980, p. 558) is incorrect.

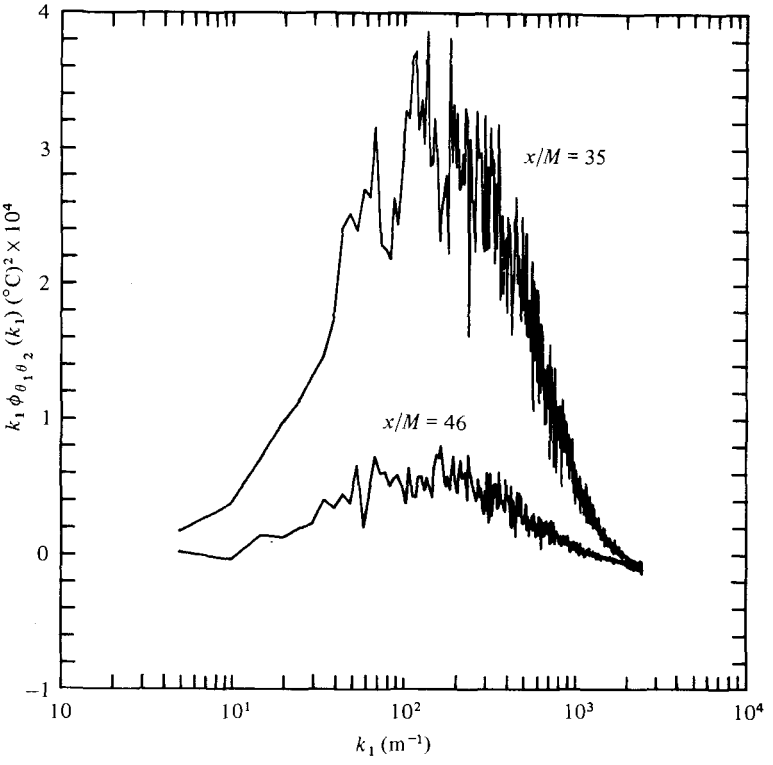

FIGURE 5. Covariance spectra at $x/M = 35$ and $x/M = 46$ for the data of figure 1 deduced by subtracting curves S from B (figures 4*a*, *b*) and dividing by 2.

superposition used here may not apply. For reference the velocity variance decay law was $\overline{u^2}/U^2 = 0{\cdot}08(x/M)^{-1{\cdot}35}$.

Figure 3 shows the power spectra of the temperature fluctuations, measured at $x/M = 35$. Shown are the spectra of each *mandoline* operating separately, their sum (S) and the spectrum of both *mandolines* operating together (B). The integral of the difference between curves B and S represents the covariance term of equation (4). Figure 4(*a*) shows the power spectra of figure 3 multiplied by wavenumber, k. This representation indicates the wavenumber at which the peak energy lies and is commonly used in the meteorological literature (Lumley & Panofsky 1964). Note that the spectra for the case when each *mandoline* is operating separately peak at different wavenumbers in accordance with their different variance decay rates and these measurements are in quantitative agreement with those of Warhaft (1980). The linear ordinate of figure 4 also accentuates the difference between curves B and S. Figure 4(*b*) shows the temperature spectra at $x/M = 46$. As x/M increases, not only does the magnitude of the spectra decrease but so also does the difference between curves B and S since the covariance is decreasing. Note also that the magnitude of the spectrum for the *mandoline* at (15, 1) is decreasing at a faster rate than the magnitude of the spectrum for the *mandoline* at (10, 2) and this is in accord with the faster variance decay for the *mandoline* at (15, 1) (figure 1). Figure 5 shows the spectra of $\overline{\theta_1\theta_2}$, for $x/M = 35$ and $x/M = 46$, derived by substracting spectrum S from spectrum B in figure 4 (and

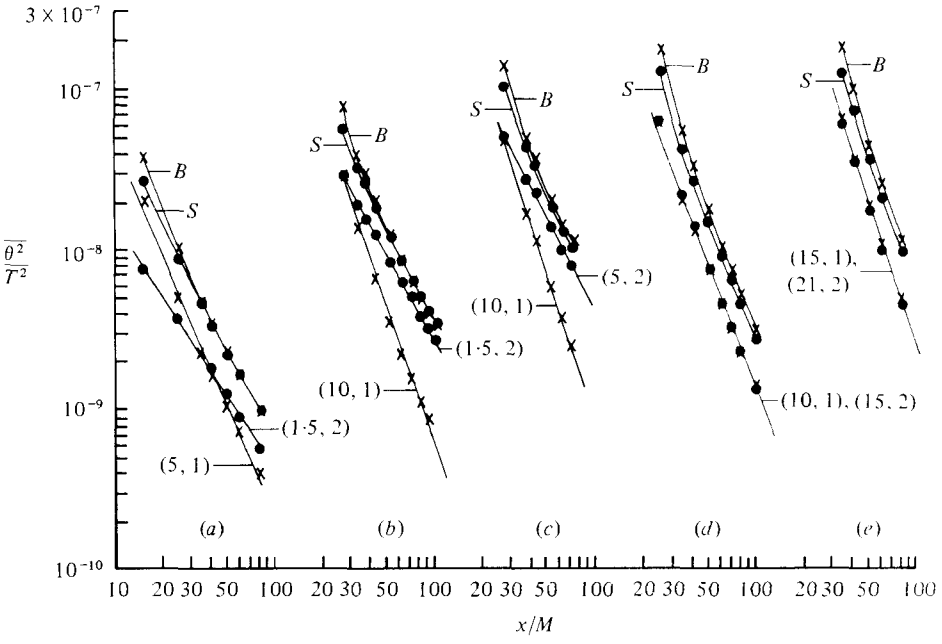

FIGURE 6. Five separate experiments of temperature variance decay for each *mandoline* heated separately, lower two curves, their sum (S) and the variance decay when both *mandolines* are heated simultaneously (B). The *mandoline* configurations for the separate experiments (a)–(e) are shown on the graphs. The data points are listed in table 1.

dividing by 2). It is of course not possible to obtain a phase spectrum since curves B and S of figure 4 were not measured simultaneously. Note that the co-spectra (figure 5) become slightly negative at high frequencies probably owing to slightly incorrect noise compensation at these frequencies.

The above experiment, then, has determined the covariance destruction rate for the case of two passive scalars for which the diffusivities are the same. A further question to be addressed, however, is, how does the covariance destruction rate and hence the rate at which the cross-correlation decays depend on the relative thermal scale sizes and the initial input locations of the two scalars?

4. Dependence of $\overline{\theta_1\theta_2}$ and ρ decay on initial conditions

Figure 6 shows five further temperature covariance decay experiments for various *mandoline* combinations (labelled on the graph) and figures 7 and 8 show the covariance and cross-correlation coefficient decays respectively, derived in the same way as those of figure 2, which are also re-plotted in figures 7 and 8. Table 1 lists the data of figures 1 and 6.

The $\overline{\theta_1\theta_2}$ decay curves of figure 7 and the ρ decay curves of figure 8 show that as the *mandolines* are progressively moved away from the grid $\overline{\theta_1\theta_2}$ and ρ decay less rapidly: for the *mandolines* at (1·5, 2) and (5, 1) and for the *mandolines* at (1·5, 2) and (10, 1) $\overline{\theta_1\theta_2}$ has a decay law exponent of $-5{\cdot}5$; for the *mandoline* configuration (5, 2) and (10, 1) the

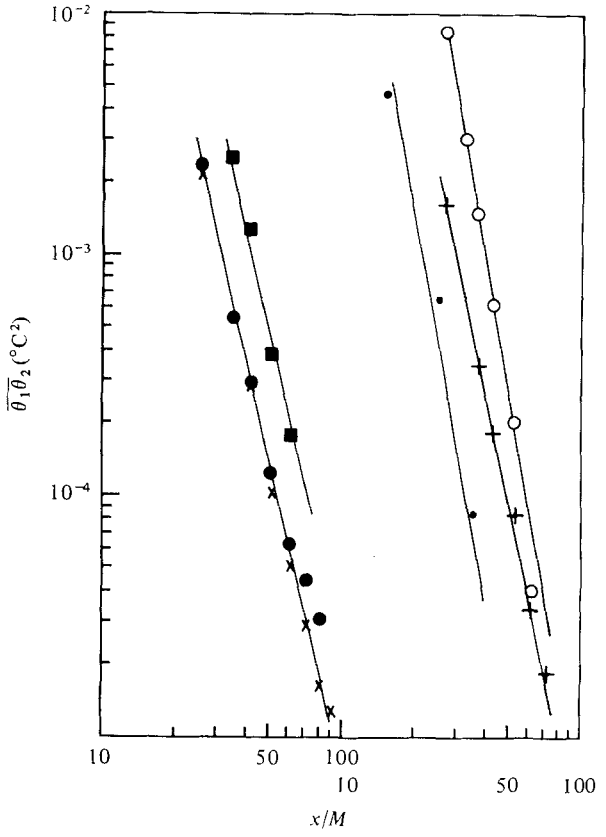

FIGURE 7. The decay of covariance, $\overline{\theta_1\theta_2}$, for all the experiments of figure 6 and the experiment of figure 1 derived in the same way as figure 2(*a*).

Mandoline configuration	Symbol
(1·5, 2) and (5, 1)	•
(1·5, 2) and (10, 1)	○
(5, 2) and (10, 1)	+
(10, 1) and (15, 2)	●
(10, 2) and (15, 1)	×
(15, 1) and (21, 2)	■

The $\overline{\theta_1\theta_2}$ decay curves for *mandoline* configurations (1·5, 2) and (5, 1) and *mandoline* configurations (1·5, 2) and (10, 1) have been multiplied by 10.

decay-law exponent is $-4{\cdot}6$; for the three experiments in which the *mandolines* were placed at $x/M \geqslant 10$ (figure 1 and figure 6*d*, *e*) the decay-law exponent has decreased to -4.

An explanation for this trend probably lies in the way turbulence evolves downstream from a grid. Initially there is a region in which the wakes behind the individual bars are coalescing; here the flow is inhomogeneous and the turbulence energy, and hence its dissipation rate, is large. It is only at many mesh lengths downstream from the grid that the homogeneous and approximately isotropic region begins to develop; this is the region in which the velocity (and thermal) variance obeys the characteristic power-law decay. Thus the fast decay of ρ and $\overline{\theta_1\theta_2}$ for the two cases when the *mando-*

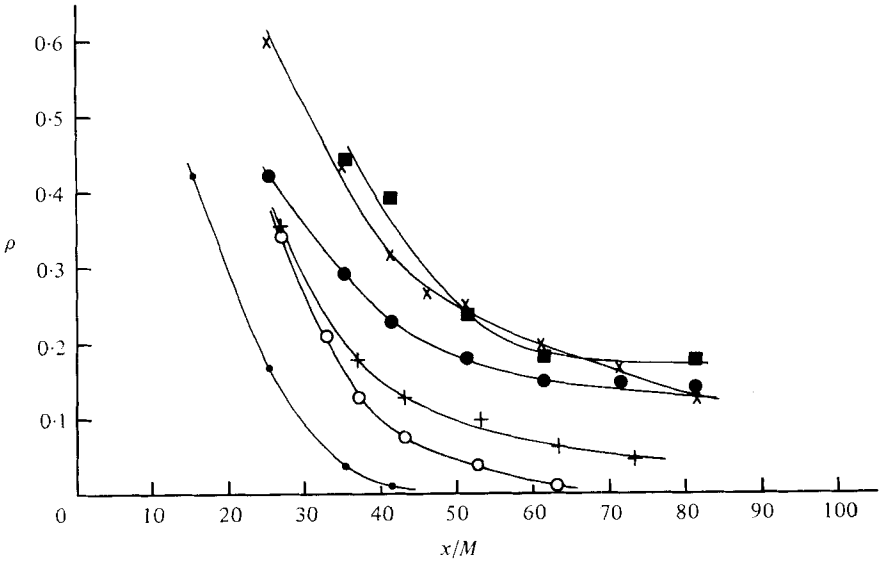

FIGURE 8. The cross-correlation coefficient, ρ, for all the experiments of figure 6 and the experiment of figure 1. The symbols represent the same *mandoline* configurations as in figure 7.

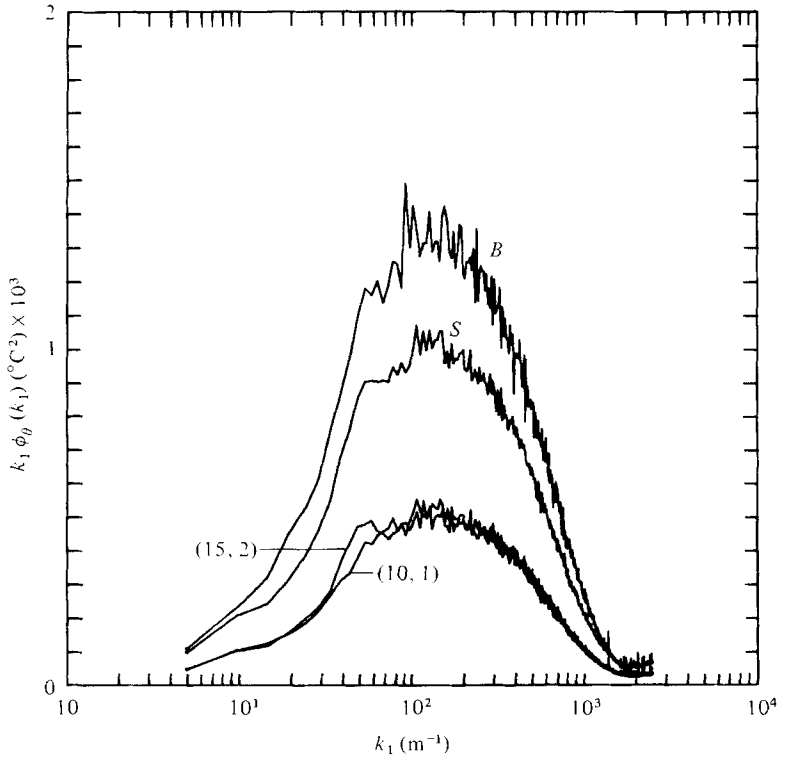

FIGURE 9. Power spectra for the *mandoline* configuration (10, 1) and (15, 2) at $x/M = 38$. The notation is the same as for figure 3.

x/M	$\overline{\theta_1^2}/T^2$	$\overline{\theta_2^2}/T^2$	$\overline{\theta_S^2}/T^2$	$\overline{\theta_B^2}/T^2$
Experiment of figure 1				
	(10, 2)	(15, 1)		
25·4	3·11	5·27	8·38	13·22
35·4	1·40	1·48	2·88	4·11
41·4	0·96	0·81	1·77	2·32
51·4	0·56	0·38	0·94	1·16
61·4	0·38	0·23	0·61	0·72
71·4	0·27	0·14	0·42	0·48
81·4	0·21	0·10	0·31	0·35
Experiment of figure 6(*b*)				
	(1·5, 2)	(10, 1)		
27	2·85	2·83	5·67	7·59
33	1·90	1·40	3·30	3·98
37	1·59	1·05	2·64	2·97
43	1·23	0·65	1·88	2·01
53	0·85	0·35	1·20	1·25
63	0·63	0·22	0·86	0·86
73	0·50	0·16	0·66	0·65
83	0·40	0·11	0·50	0·50
Experiment of figure 6(*d*)				
	(10, 1)	(15, 2)		
25·4	6·38	6·23	12·52	17·78
35·4	2·18	2·07	4·24	5·47
41·4	1·40	1·34	2·74	3·39
51·4	0·77	0·76	1·53	1·80
61·4	0·47	0·48	0·95	1·09
71·4	0·33	0·33	0·66	0·76
81·4	0·24	0·24	0·48	0·54

x/M	$\overline{\theta_1^2}/T^2$	$\overline{\theta_2^2}/T^2$	$\overline{\theta_S^2}/T^2$	$\overline{\theta_B^2}/T^2$
Experiment of figure 6(*a*)				
	(1·5, 2)	(5, 1)		
15·4	0·76	2·01	2·77	3·80
25·4	0·38	0·51	0·89	1·03
35·4	0·24	0·24	0·47	0·49
41·4	0·18	0·17	0·35	0·35
51·4	0·13	0·11	0·24	0·24
61·4	0·092	0·074	0·17	0·17
81·4	0·058	0·040	0·098	0·10
Experiment of figure 6(*c*)				
	(5, 2)	(10, 1)		
27	5·38	5·06	10·45	14·21
37	2·82	1·75	4·57	5·36
43	2·34	1·12	3·46	3·87
53	1·41	0·59	2·00	2·19
63	1·01	0·38	1·40	1·47
73	0·80	0·25	1·10	1·14
—	—	—	—	—
—	—	—	—	—
Experiment of figure 6(*e*)				
	(15, 1)	(21, 2)		
35·4	6·15	6·50	12·66	18·28
41·4	3·64	3·69	7·33	10·18
51·4	1·80	1·88	3·68	4·55
61·4	1·04	1·11	2·15	2·54
81·4	0·48	0·51	0·98	1·16
—	—	—	—	—
—	—	—	—	—

TABLE 1. Tabulation of the data of figures 1 and 6. Subscripts S and B have same meaning as in the figures. All values are $\times 10^8$. $T = 300$ K.

lines are placed close to the grid (configurations (1·5, 2) and (5, 1) and configurations (1·5, 2) and (10, 1)) may be attributable to the very rapid mixing of the scalars by the intense velocity fluctuations in this region. Further downstream the velocity fluctuations are less intense and thus less rapid mixing of the scalars would be expected if they are injected here. Thus the decay rate of $\overline{\theta_1\theta_2}$ and ρ should decrease, as is observed.

We note that for all the above experiments the two scalars were injected at different longitudinal positions downstream from the grid. The cases where both the scalars are injected at the same position from the grid, and particularly very close to the grid (a case pertinent to the practical situation of chemical mixing), will be discussed in a future publication where the inference method described here will also be compared and corroborated with a direct method in which two different scalars (temperature and helium) are used.

Figure 9 shows the spectra measured at $x/M = 38$ for the *mandolines* at (10, 1) and (15, 2) and here we see that the two spectra, for the *mandolines* heated separately, peak at the same wavenumber in accord with their similar decay rates (figure 6*d*). In this

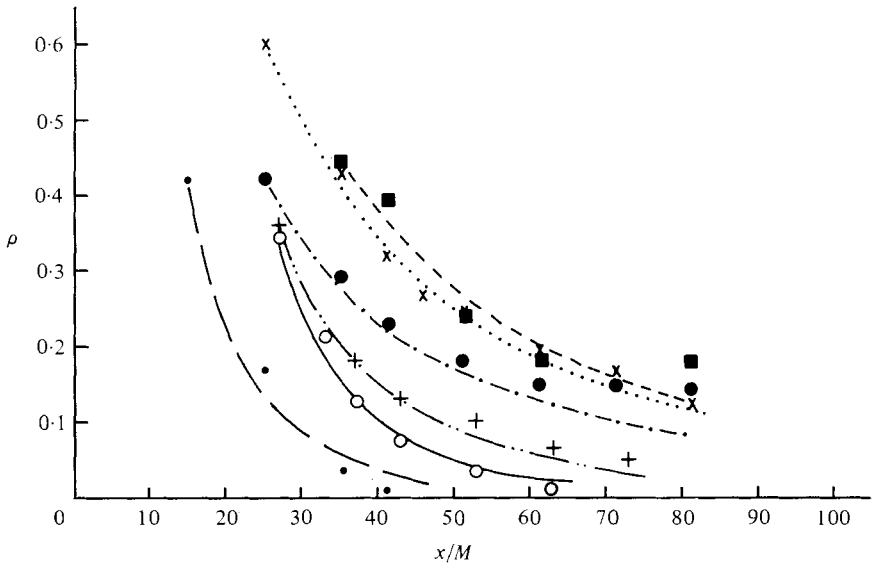

FIGURE 10. Equation (10) fitted to the ρ decay curves.

Mandoline configuration	Symbol (experimental data)	Coefficient C (equation (7))	Solution of equation (7)
(1·5, 2) and (5, 1)	•	1·4	——
(1·5, 2) and (10, 1)	○	1·4	——
(5, 2) and (10, 1)	+	1·0	—··—
(10, 1) and (15, 2)	●	0·55	—·—
(10, 2) and (15, 1)	×	0·55	.....
(15, 1) and (21,2)	■	0·55	– – –

experiment we have exactly compensated the decrease in thermal length scale obtained as the *mandoline* is moved further from the grid by increasing the spacing of the wires and thus the *mandoline* at (15, 2) gives the same variance decay rate and thermal length scale as the *mandoline* at (10, 1). (The same situation applies also to the experiment of figure 6(*e*).) The spectra of figure 10 should be contrasted with those of figure 4(*a*) where the *mandolines* were placed at the same locations but in reverse order, i.e. at (10, 2) and (15, 1). For this situation the spectra peak at different wavenumbers and the thermal variance decays are different. We note however that although both the relative and absolute thermal input scales are different for the two cases (figures 4*a* and 10) the decay rate of the thermal covariance is the same, with a decay exponent of -4 (figure 7).

5. Modelling the decay rate of ρ

In analogy to the way we model the rate equation for a scalar variance (Tennekes & Lumley 1972) viz.

$$\dot{\overline{\theta^2}} = 6\kappa\overline{\theta^2}/\lambda_\theta^2, \tag{5}$$

where the dot indicates differentiation with respect to time and λ_θ is the scalar Taylor microscale, a reasonable assumption for the scalar co-variance rate equation would be

$$\dot{\overline{\theta_1\theta_2}} = \text{fn}\,(\kappa, \overline{\theta_1^2}, \overline{\theta_2^2}, \lambda_{\theta_1}, \lambda_{\theta_2}, \rho). \tag{6}$$

Dimensional reasoning alone, however, will not provide a unique combination for equation (6), for example $\overline{\theta_1^2}/\lambda_{\theta_1}^2$ and $\overline{\theta_2^2}/\lambda_{\theta_2}^2$ could appear multiplicatively or additively (with suitable exponents); alternative simple combinations do not exist for equation (5). Furthermore the two thermal Taylor microscales may have a variable cross-correlation, adding another term to equation (6). Clearly more subtle considerations are necessary.

Lumley (1978*a*) has examined such problems using second-order closure techniques (sometimes called one-point closure). The reader is referred to his paper for a detailed survey of the technique. Here it will suffice to state that second-order modelling, which aims to predict integrated quantities such as variances and correlation coefficients, is a scheme for closing the second-order equations (such as equation (1)) by modelling third-order quantities in terms of second-order quantities. Two vital aspects of the modelling procedure are that the model equations must have the correct invariance characteristics and that a set of realizability conditions must be fulfilled; an example of this latter aspect is that if a non-negative quantity approaches zero then so must its derivative. The realizability condition has often been neglected by previous workers.

Using the above technique, Lumley (1978*b*) shows that for two scalars in decaying turbulence

$$\dot{\rho}/\rho = -C(\epsilon_{\theta_1}/\overline{\theta_1^2} + \epsilon_{\theta_2}/\overline{\theta_2^2})\,(1-\rho^2), \tag{7}$$

where ϵ_{θ_1}, and ϵ_{θ_2} are the dissipation rates of the thermal variances of $\overline{\theta_1^2}$ and $\overline{\theta_2^2}$ respectively. The constant C must be determined from experiment. Note that the terms $\epsilon_\theta/\overline{\theta^2}$, which are inverse time scales, appear in additive rather than multiplicative form; the later combination does not fulfil realizability conditions (Lumley, personal communication). Note also that the $1-\rho^2$ term in equation (7) shows that if the initial scalar cross-correlation is unity then it will always remain unity, i.e. the scalars will not decouple. This, of course, is physically correct since if two perfectly correlated scalars of the same diffusivity are added to a flow there is no mechanism by which they will be decoupled. If, however, the scalars had significantly different diffusivities, then, even if their cross-correlation were initially unity, they would decouple and equation (7) would not hold.

For the individual $\overline{\theta^2}$ decay of figure 6 which can be described well in terms of a power-law decay

$$\overline{\theta^2} = A(x/M)^{-m}, \tag{8}$$

where A and m are constants for each experiment,

$$\begin{aligned} \epsilon_\theta &= -\tfrac{1}{2}(d\overline{\theta^2}/dt), \\ &= \frac{UmA}{2M}\left(\frac{x}{M}\right)^{-m-1}, \end{aligned} \tag{9}$$

thus equation (7) reduces to

$$\dot{\rho}/\rho = -C\frac{U}{2M}\left(\frac{x}{M}\right)^{-1}(m_1+m_2)\,(1-\rho^2). \tag{10}$$

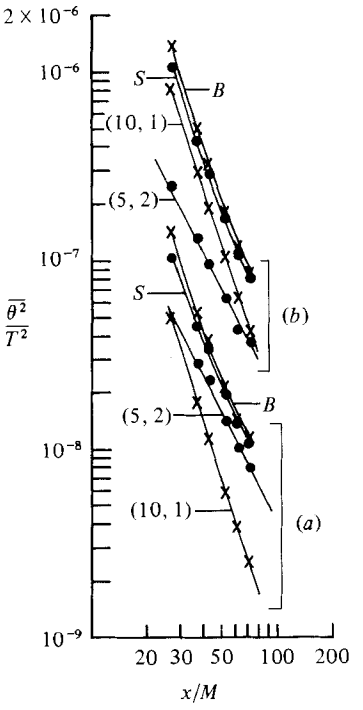

FIGURE 11. Two different realizations of temperature variance and covariance decay for the *mandolines* at (5, 2) and (10, 1). The notation is the same as figure 1. Curves (*a*) are the same as figure 6(*c*).

Here m_1 and m_2 are the decay exponents for the individual thermal variance decays of each two *mandoline* experiments.

For all the experiments of figure 6, as well as for the experiment of figure 1, equation (10) has been solved using the values of m_1 and m_2 taken from these figures. The initial condition has been the initial value of ρ taken from figure 8 for each trial. The results are plotted in figure 10. A good fit to the data points is achieved if C (equation (10)) is taken as 1·4 for the two cases where the *mandolines* are close to the grid (experiments (*a*) and (*b*) of figure 6) and if $C = 0{\cdot}55$ for the cases where the *mandolines* are placed at $x/M \geqslant 10$ (experiments (*d*) and (*e*) of figure 6 and the experiment of figure 1). For the intermediate case (*mandolines* at (5, 2) and (10, 1)), C has been taken as 1. Thus, although equation (7) fits the form of the ρ decay data well, the (relatively small) variation of the constant C suggests that the equation requires some modification in order to eliminate this variation.

Finally, it should be noted that a decay law $\dot{\rho}/\rho \propto (x/M)^{-1}$ immediately follows if it is assumed that $\overline{\theta_1 \theta_2}$ has a power-law decay; the model outlined here, however, only makes assumptions concerning the decay of the scalar variances. Furthermore, the above model predicts the $1-\rho^2$ term, which has important physical significance as mentioned above.

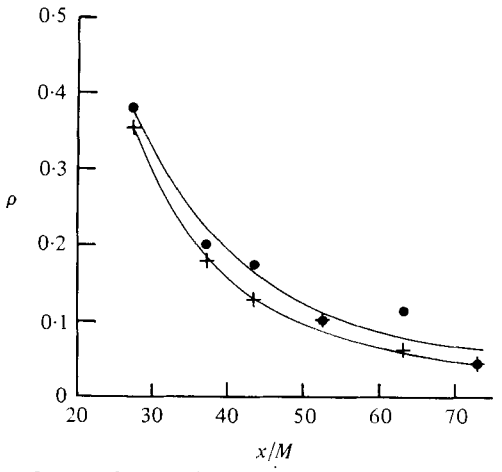

FIGURE 12. The decay of ρ for the two realizations of figure 11: +, (*a*); ●, (*b*).

6. Discussion of method

The method of inferring the cross-correlation between θ_1 and θ_2 relies on the assumption that the thermal fluctuations from the first *mandoline* do not interfere with the production of thermal fluctuations from the second *mandoline*, i.e. $\overline{\theta_2^2}$ is the same whether the first *mandoline* is operating or not. While we cannot formally prove that there is no interference, we will present a number of points that suggest there is none. First, the form of the covariance and cross-correlation decays of figures 7 and 8 were independent of both the relative values and the absolute values of the current fed through the *mandoline* wires. Figure 11 shows two trials done for the *mandoline* configuration (5, 2) and (10, 1). For figure 11 (*a*) (the same as figure 6*c*) the current in the two *mandolines* was adjusted so that the thermal variance from each *mandoline* was the same at $x/M = 27$ while for figure 11 (*b*) the current was adjusted so that at $x/M = 27$ $\overline{\theta^2}$ was 3·5 times greater for the *mandoline* at (10, 1) than for the *mandoline* at (5, 2) and their variances became equal only at about $x/M = 80$. Furthermore, the absolute variances were different by a factor of approximately 10 for the two cases. However, ρ inferred from these two trials (figure 12) was essentially the same. It would be expected that if $\overline{\theta_2^2}$ was dependent on $\overline{\theta_1^2}$ then if $\overline{\theta_1^2}$ were changed relative to $\overline{\theta_2^2}$ some effect would be seen on the ρ decay. Secondly, consider the two experiments in which the *mandoline* configurations were (10, 2) and (15, 1) (figure 1) and then (10, 1) and (15, 2) (figure 6*d*). In the first experiment the *mandoline* with one mesh spacing was placed after the *mandoline* with two mesh spacings and then the *mandolines* were reversed, the *mandoline* with two mesh spacings was placed after the *mandoline* with one mesh spacing. If there was an interference effect from the upstream *mandoline* it would be reasonable to expect that it be a function of the wire spacings (and hence of the thermal scale of θ_1) yet for both these experiments the same covariance and ρ decay forms were observed. Thirdly, the temperature of the *mandoline* wires is approximately 230 °C (Warhaft 1980) while the r.m.s. temperature of the fluctuations from the first *mandoline* when they reach the second *mandoline* is typicically 0·1 °C and their mean temperature is

approximately 27° C (ambient temperature). It is doubtful that these small fluctuations would influence the heat released from the second *mandoline* wires which are over 200 °C above ambient temperature. These three reasons suggest, then, that it is highly unlikely that the θ_1 fluctuations affect the production of the θ_2 fluctuations.

7. Concluding remarks

A simple method by which scalar covariance decay is inferred by the injection of a single scalar at two separate locations into decaying grid turbulence has been described. The results show that the scalar covariance follows a power-law decay, the exponent varying from $-5{\cdot}5$ if both *mandolines* are placed close to the grid to -4 if the two scalars are introduced further downstream ($x/M \geqslant 10$). While the decay rate of $\overline{\theta_1\theta_2}$ decreases as the *mandolines* are placed further downstream (in contrast, it should be noted, to the variance decay rate which increases as the *mandolines* are placed further downstream) its decay seems to be less sensitive to initial conditions than that of the variance decay. Thus in the region $x/M \geqslant 10$, three experiments in which the *mandoline* configurations were different gave the same covariance decay rate, with a power-law exponent of -4.

Finally, it should be pointed out that since the destruction rate of the scalar covariance indicates the rate at which the turbulent fluctuations mix the scalars the method employed here could be used for the investigation of other, more complex flows, such as jets and wakes, so long as they are statistically stationary.

I wish to thank Professor J. L. Lumley for continued encouragement and discussions concerning second-order modelling. I also wish to thank Mr E. P. Jordan and Mr A. Sirivat for technical assistance and Professors S. Corrsin and C. Van Atta for helpful comments on the original manuscript.

This work was funded by grants from the Atmospheric Science section and the Engineering section of the U.S. National Science Foundation. The respective grant numbers are ATN77-22903 and ENG 7822100.

REFERENCES

Corrsin, S. 1961 Some statistical properties of the product of a turbulent, first order reaction. *Proc. Symp. on Fluid Dynamics and Applied Math., Univ. Maryland.* Gordon and Breach.

Hill, J. C. 1976 Homogeneous turbulent mixing with chemical reaction. *Ann. Rev. Fluid Mech.* **8**, 135–162.

Libby, P. A. & Williams, F. A. 1976 Turbulent flows involving chemical reactions. *Ann. Rev. Fluid Mech.* **8**, 351–376.

Lumley, J. L. 1978*a* Computational modelling of turbulent flows. *Advances in Applied Mechanics*, vol. 18 (ed. C.-S. Yih), pp. 123–176. Academic.

Lumley, J. L. 1978*b* Turbulent transport of passive contaminants and particles: fundamental and advanced methods of numerical modelling. *Lecture Series* 1977–8, *Pollutant Dispersal.* Von Kármán Institute for Fluid Dynamics, Rhode-St.-Genese, Belgium.

Lumley, J. L. & Panofsky, H. A. 1964 *The Structure of Atmospheric Turbulence.* Academic.

Tennekes, H. & Lumley, J. L. 1972 *A First Course in Turbulence.* Massachusetts Institute of Technology Press.

Warhaft, Z. 1976 Heat and moisture flux in the stratified boundary layer. *Quart. J. Roy. Met. Soc.* **102**, 703–707.

WARHAFT, Z. 1980 A experimental study of the effect of uniform strain on thermal fluctuations in grid generated turbulence. *J. Fluid Mech.* **99**, 545–573.

WARHAFT, Z. & LUMLEY, J. L. 1978 An experimental study of the decay of temperature fluctuations in grid generated turbulence. *J. Fluid Mech.* **88**, 659–684.

WYNGAARD, J. C., PENNELL, W. T., LENSCHOW, D. H. & LEMONE, M. A. 1978 The temperature–humidity covariance budget in the convective boundary layer. *J. Atmos. Sci.* **35**, 47–58.